Neurotherapeutics 21 (2024) e00372

Contents lists available at ScienceDirect

Neurotherapeutics

journal homepage: www.sciencedirect.com/journal/neurotherapeutics

Original Article

Amelioration of functional and histopathological consequences after spinal cord injury through phosphodiesterase 4D (PDE4D) inhibition

Melissa Schepers [a,b,c,1], Sven Hendrix [d,1], Femke Mussen [a,b,e,1], Elise van Breedam [f], Peter Ponsaerts [f], Stefanie Lemmens [e], Niels Hellings [c,e], Roberta Ricciarelli [g,h], Ernesto Fedele [g,i], Olga Bruno [j], Chiara Brullo [j], Jos Prickaerts [k], Jana Van Broeckhoven [c,e,2], Tim Vanmierlo [a,b,c,*,2]

[a] Department of Neuroscience, Biomedical Research Institute, Faculty of Medicine and Life Sciences, Hasselt University, 3500 Hasselt, Belgium
[b] Department of Psychiatry and Neuropsychology, School for Mental Health and Neuroscience, Maastricht University, 6229ER Maastricht, the Netherlands
[c] University MS Centre (UMSC) Hasselt – Pelt, Belgium
[d] Institute for Translational Medicine, Medical School Hamburg, 20457 Hamburg, Germany
[e] Department of Immunology and Infection, Biomedical Research Institute, Faculty of Medicine and Life Sciences, Hasselt University, 3500 Hasselt, Belgium
[f] Laboratory of Experimental Hematology, Vaccine and Infectious Disease Institute (Vaxinfectio), University of Antwerp, 2610 Wilrijk, Belgium
[g] IRCCS Ospedale Policlinico San Martino, 16100 Genoa, Italy
[h] Department of Experimental Medicine, Section of General Pathology, University of Genova, 16100 Genoa, Italy
[i] Department of Pharmacy, Section of Pharmacology and Toxicology, University of Genoa, 16100 Genoa, Italy
[j] Department of Pharmacy, Section of Medicinal Chemistry, University of Genoa, 16100 Genoa, Italy
[k] Peitho Translational, 6229ER Maastricht, the Netherlands

ARTICLE INFO

Keywords:
Spinal cord injury
Phosphodiesterase 4
cAMP
Neuroinflammation
Regeneration

ABSTRACT

Spinal cord injury (SCI) is a life-changing event that severely impacts the patient's quality of life. Modulating neuroinflammation, which exacerbates the primary injury, and stimulating neuro-regenerative repair mechanisms are key strategies to improve functional recovery. Cyclic adenosine monophosphate (cAMP) is a second messenger crucially involved in both processes. Following SCI, intracellular levels of cAMP are known to decrease over time. Therefore, preventing cAMP degradation represents a promising strategy to suppress inflammation while stimulating regeneration. Intracellular cAMP levels are controlled by its hydrolyzing enzymes phosphodiesterases (PDEs). The PDE4 family is most abundantly expressed in the central nervous system (CNS) and its inhibition has been shown to be therapeutically relevant for managing SCI pathology. Unfortunately, the use of full PDE4 inhibitors at therapeutic doses is associated with severe emetic side effects, hampering their translation toward clinical applications. Therefore, in this study, we evaluated the effect of inhibiting specific PDE4 subtypes (PDE4B and PDE4D) on inflammatory and regenerative processes following SCI, as inhibitors selective for these subtypes have been demonstrated to be well-tolerated. We reveal that administration of the PDE4D inhibitor Gebr32a, even when starting 2 dpi, but not the PDE4B inhibitor A33, improved functional as well as histopathological outcomes after SCI, comparable to results obtained with the full PDE4 inhibitor roflumilast. Furthermore, using a luminescent human iPSC-derived neurospheroid model, we show that PDE4D inhibition stabilizes neural viability by preventing apoptosis and stimulating neuronal differentiation. These findings strongly suggest that specific PDE4D inhibition offers a novel therapeutic approach for SCI.

Introduction

Spinal cord injury (SCI) is characterized by a complex secondary injury phase that drives further permanent damage and causes neurological dysfunction [1,2]. To date, regeneration and recovery of function remain limited after SCI [3]. The provoked neuroinflammation and the limited endogenous regeneration potential of neural tissue are the critical bottlenecks. Despite multiple efforts, current treatments suppress inflammatory processes (e.g. corticosteroids) but remain ineffective in promoting repair. Therefore, there is an urgent need to develop new

* Corresponding author.
E-mail address: t.vanmierlo@maastrichtuniversity.nl (T. Vanmierlo).
[1] Equally contributing first authors.
[2] Equally contributing last authors.

https://doi.org/10.1016/j.neurot.2024.e00372
Received 15 December 2023; Received in revised form 15 April 2024; Accepted 1 May 2024

therapeutic strategies that tackle both neuroinflammatory and regenerative processes.

Cyclic adenosine monophosphate (cAMP) is a crucial molecule involved as a second messenger in multiple signaling pathways and exerts broad modulatory effects in various cell types [4,5]. In the context of central nervous system (CNS) injury, cAMP has been shown to exhibit both anti-inflammatory and neuroregenerative functions. Upon SCI, cAMP levels in both neurons and glial cells decrease dramatically [6]. Therefore, maintaining or elevating the intracellular cAMP levels to regulate the immune responses or to stimulate neuroregeneration can be considered a valuable approach to temper SCI pathogenesis. Phosphodiesterases (PDEs) are a class of enzymes responsible for the degradation of cyclic nucleotides, such as cAMP. In the CNS, PDE4 is primarily responsible for the breakdown of cAMP [4,7]. As such, PDE4 inhibition, initiated after SCI induction, demonstrated a wide range of beneficial actions in a SCI mouse model [8–12]. The golden standard, first-generation PDE4 inhibitor rolipram was found to act as anti-inflammatory, neuroprotective, and regenerative agent [9–11]. Continuous and controlled mini-osmotic pump-mediated release of rolipram (0.4 μmol/kg/h) attenuated astrogliosis and enhanced axonal outgrowth following hemisection SCI, while administration of a single dose of 0.5 or 1 mg/kg rolipram per day appeared to be sufficient to enhance neuronal survival and simultaneously protect oligodendrocytes, thus preserving CNS myelination following contusion SCI [9–11]. Additionally, the PDE4 inhibitor IC486051 further confirmed the anti-inflammatory properties observed upon rolipram administration as bolus doses of 0.5 or 1.0 mg/kg IC486051 decreased oxidative stress markers and leukocyte infiltration into the lesion size, thereby reducing the resulting tissue damage following compression SCI in Wistar rats [8]. However, despite these promising findings, the clinical translation of pan PDE4 inhibitors has been hampered due to tolerability problems (e.g., emesis). Therefore, to mitigate the side effects and increase tolerability, PDE4 subtype-selective inhibitors have been developed. The PDE4 family consists of four genes yielding different PDE4 subtypes (PDE4A-PDE4D). PDE4A, B, and D are widely expressed in the CNS of rodents and humans, while PDE4C has limited CNS expression. In particular, the PDE4B and PDE4D subtypes recently gained more interest in neurological disorders because of their anti-inflammatory and neuroplastic effects, respectively [13–15]. More specifically, the inhibition of PDE4B suppresses the neuroinflammatory responses of macrophages and microglia, while PDE4D blockage has been shown to successfully boost myelin regeneration and enhance neuroplasticity [14–18]. Targeting these individual subtypes circumvented the emetic side-effects accompanied by pan PDE4 inhibitors such as roflumilast and rolipram, and is predicted as a valuable strategy to target neuroinflammation [19].

In this study, we aimed to disentangle the effect of PDE4B and PDE4D inhibition on SCI pathology. Using the SCI hemisection model, we show in mice that, in contrast to the PDE4B inhibitor A33, the PDE4D inhibitor Gebr32a improved functional and histopathological outcomes after SCI to a similar extent as the pan PDE4 inhibitor roflumilast. Gebr32a could still improve SCI outcomes even when administered 2 dpi. *In vitro*, neuronal apoptosis was prevented by inhibiting PDE4D, as demonstrated with primary neuronal mouse cultures, human iPSC-derived neuronal precursor cultures, and luminescent iPSC-derived neurospheroids. In addition, increased neuronal differentiation was observed in these iPSC-derived neurospheroids. Overall, these findings underline the therapeutic potential of specific PDE4D inhibition to act neuroprotective and consequently improve neural plasticity, leading to functional recovery after SCI.

Methods

Animals

In vivo experiments were performed with 10- to 12-week-old female WT C57BL/6j mice (Janvier Labs). Mice were housed in groups at the conventional animal facility of Hasselt University under stable conditions (temperature-controlled room, 12 h light/dark cycle, food, and water *ad libitum*). Experiments were approved by the local ethical committee of Hasselt University (ethical ID 202060) and were performed according to the guidelines of Directive 2010/63/EU on the protection of animals used for scientific purposes.

Spinal cord injury model

A standardized T-cut spinal cord hemisection injury was performed as previously described [20–22]. In brief, mice were anesthetized with 2–3% isoflurane and a partial laminectomy was performed at thoracic level 8. A bilateral hemisection injury was done using iridectomy scissors to transect the dorsomedial and ventral corticospinal tract. Afterward, the back muscles were sutured, and the skin was closed with wound clips (Bioconnect). Post-operative treatment included blood-loss compensation by glucose solution (20%, intraperitoneal [i.p.]) and pain relief by buprenorphine (0.1 mg/kg body weight, Temgesic, subcutaneous [s.c.]). In addition, mice were placed in a heated recovery chamber (33 °C) until they regained consciousness. Bladders were voided daily until the micturition reflex was restored spontaneously. The *in vivo* experiments were conducted in two independent cohorts. Table 1 provides a sample size overview for each experimental animal group for both cohorts.

Animal treatments

Starting 1 h after SCI, mice were injected twice daily s.c. for 28 days with either (1) vehicle (0.1% DMSO (VWR prolabo) + 0.5% methylcellulose + 2% Tween80), (2) the pan PDE4 inhibitor roflumilast (3 mg/kg, Xi'an leader biochemical engineering co., LTD), (3) the PDE4B inhibitor A33 (3 mg/kg, Sigma-Aldrich), or (4) the PDE4D inhibitor Gebr32a (0.3 mg/kg, University of Genoa [23]). We included (5) a sequential treatment group who first received A33 (3 mg/kg) until 10 days post injury (dpi), followed by Gebr32a (0.3 mg/kg) until the end of the experiment (injection volume: 10 μl/g body weight). This treatment was used to first diminish the acute inflammatory responses with PDE4B inhibition in the early phase, followed by PDE4D inhibition later to boost endogenous repair mechanisms and hence, promote SCI recovery by tackling both the inflammatory and repair processes. Lastly, we elucidated the therapeutic potential of Gebr32a when administered in a more clinically relevant therapeutic window. To this purpose, mice were injected twice daily s.c. for 28 days with (1) vehicle (0.1% DMSO) or Gebr32a (0.3 mg/kg) starting from (2) 2 dpi or (3) 10 dpi onwards.

Locomotion test

Following SCI, functional recovery was assessed using the standardized Basso Mouse Scale (BMS) score for locomotion [24]. This 10-point scale ranges from 0, indicating complete hind limb paralysis, to 9, representing normal motor function. These scores are based on hind limb movements in an open field during a 4 min testing window. The

Table 1
Overview of the number of animals receiving a hemisection SCI which were included in cohort 1 and cohort 2 for functional and histopathological analysis based on locomotor function. The A33 and Gebr32a sequential treatment group was not included in cohort 2 due to the lack of additional efficacy compared to continuous PDE4D inhibition.

Treatment group	Number of animals		
	Included cohort 1	Included cohort 2	Total
Vehicle	6	9	15
Roflumilast (3 mg/kg)	7	7	14
A33 (3 mg/kg)	6	10	16
Gebr32a (0.3 mg/kg)	8	6	14
A33 followed by Gebr32a	10	/	10

evaluation was done by an investigator blinded to treatment groups and was performed daily from 1 until 7 dpi, followed by a scoring every 2–3 days until the end of the experiment (28 dpi). The mean BMS score of the left and right hind limb was used per animal. Mice were excluded from the analysis if 1) they had a BMS score higher than 1 at 1 dpi or 2) they did not show an increase in BMS score of at least 1 point at 28 dpi.

Mouse primary neuronal cultures

Fetal mice brains (E16-19) were used to obtain primary cortical neuron cultures [25]. Meninges-free cerebral cortices were chemically dissociated for 15 min using trypsin. Next, chemical dissociation was stopped by washing cortices with minimal essential medium (MEM) supplemented with 1% heat-inactivated horse serum (Thermo Fisher), 0.6% glucose (Sigma-Aldrich) and 100 U/ml penicillin/streptomycin (Life Technologies). The cortical tissue was subsequentially mechanically dissociated with a P1000 pipette to generate single-cell suspensions. Primary mouse neurons were seeded (8×10^4 cells/well) in a poly--L-lysine (PLL, Sigma) coated 96-well plate (flat bottom, Greiner) in MEM supplemented medium. After allowing attachment for 4 h, plating MEM medium was replaced by neurobasal medium supplemented with 1× B27 supplement (Thermo Fisher), 2 mM L-glutamine (Thermo Fisher), and 100 U/ml penicillin/streptomycin (Life Technologies). Cells were maintained at 37 °C with 5% CO_2 culture conditions. Treatment (vehicle: 0.1% DMSO; roflumilast: 1 μM; A33: 1 μM; Gebr32a: 1 μM) was started 24 h after isolation, under growth factor B27 deprivation to induce neuronal cell death (an additional 48 h).

Propidium iodide (PI) viability assay

The viability of mouse primary neurons was assessed using a propidium iodide (PI) viability assay as described previously [26,27]. Briefly, 48 h after B27 growth factor deprivation and PDE inhibitor treatment, culture medium was replaced with Lysis buffer A100 (ChemoMetec) and lysis reaction was then halted by adding equal amounts of stabilization buffer B (ChemoMetec), supplemented with PI (10 μg/ml, Sigma). After 15 min incubation in the dark, fluorescent emission was measured using the FluoStart OPTIMA plate reader (Bottom-up, excitation: 540 nm; emission: 612 nm).

Luminescent iPSC-derived neurospheroid cultures

Neurospheroids were formed as described previously [28]. Briefly, eGFP/Luc human iPSC-NSCs were seeded at equal densities of 1.6×10^4 cells per well (ULA 96-well plate (Corning)) in neural expansion medium (NEM, Gibco). Neurospheroids were maintained at 37 °C, 5% CO_2 culture conditions under constant orbital shaking (85 rpm). Two days after plating, fresh NEM was added. A 50% medium change was conducted every other day. Additionally, the luminescent signal was measured weekly by adding 1.5 mg/ml Beetle luciferin (E1601, Promega) for 48 h to the neurospheroid cultures. The luminescent signal was measured using the Clariostar Plus plate reader, after which a complete medium change was performed to eliminate remaining luciferin. On the same day of bioluminescence evaluation, phase contrast pictures (4× magnification) of every neurospheroid were taken using the Incucyte system to evaluate overall neurospheroid size. The size of each neurospheroid was determined using Image J by manually delineating the spheroids. PDE inhibition treatment (vehicle: 0.1% DMSO; roflumilast: 1 μM; A33: 1 μM; Gebr32a: 1 μM) was initiated following 1 week of culturing (after the first luminescent signal measurement). At the end of the experiment (6 weeks of culturing), neurospheroids were fixed with 4% paraformaldehyde (PFA) for 150 min at room temperature (RT), incubated overnight in 20% sucrose (w/v in 1× phosphate-buffered saline [PBS]) and consecutively used for cryosectioning and immunocytochemical analysis.

Immunofluorescence

Post-mortem spinal cord tissue

At 28 dpi, mice received an overdose of i.p. dolethal (200 mg/kg) (Vetiquinol B.V.) and were transcardially perfused with Ringer solution containing heparin (50 units/l), followed by a 4% PFA in 1xPBS perfusion [29]. Longitudinal spinal cord cryosections of 10 μm thickness were obtained. Immunofluorescent staining was performed as described previously [2,3]. In brief, sections were blocked using 10% protein block (Dako) in PBS containing 0.5% Triton-X-100 for 1 h at RT. For evaluating oligodendrocyte differentiation using Olig2 and CC1, an additional antigen retrieval step using a sodium citrate buffer (10 mM Sodium citrate, 0.05% Tween20, pH 6.0) was conducted. Primary antibodies were diluted in PBS with 1% protein block and 0.5% Triton-X-100 and were incubated overnight at 4 °C (Table 2). Following washing, secondary antibody incubation was done for 1 h at RT. Antibodies used were: goat anti-rat Alexa fluor 488 (1:250, A11006, ThermoFisher Scientific), goat anti-mouse Alexa fluor 568 (1:250, A11004, ThermoFisher Scientific), goat anti-rat Alexa fluor 568 (1:250, A11077, Invitrogen), and goat anti-rabbit Alexa 488 (1:250, A11008, Invitrogen). Specificity of secondary antibodies was tested by omitting the primary antibody. Counterstaining with DAPI (1:1000, Sigma-Aldrich) was performed for 10 min. Pictures were taken using a LEICA DM4000 B LED microscope and LAS X software (Leica).

Neurospheroids

After fixation, neurospheroids were processed as described previously to allow high-throughput staining [28]. Briefly, a silicone mold with 66 wells corresponding to the size of the neurospheroids was filled with Tissue-Tek-OCT (VWR). Single neurospheroids were loaded into separate wells of the silicone mold. Next, the mold was snap-frozen in isopentane at a fixed temperature (−50 °C), after which the resulting OCT-block was removed from the silicon mold, turned upside down and covered with additional OCT before freezing a second time. Cryosections of 10 μm were obtained on PLL-coated glass slides. For immunocytochemical

Table 2
List of primary antibodies used in immunofluorescence experiments.

Immunofluorescence	Antibody	Host	Source	Dilution factor
Immunohistochemistry	GFAP	Mouse	Sigma Aldrich (**G3893**)	1/500
	MBP	Rat	Merck Millipore (**MAB386**)	1/250
	CD4	Rat	BD Biosciences (**553043**)	1/250
	Cleaved caspase 3	Rabbit	Cell signaling (**9661**)	1/100
	NeuN	Mouse	Merck Millipore (**MAB377**)	1/1000
	Olig2	Goat	Biotechne R&D (**AF2418**)	1/50
	APC (CC1)	Mouse	Calbiochem (**OP80**)	1/50
	5HT	Rabbit	Immunostar **(20080)**	1/1000
Immunocytochemistry	NeuN	Guinea-pig	Merck Millipore (**ABN90P**)	1/100
	Cleaved caspase 3	Rabbit	Cell signaling (**9661**)	1/400
	Doublecortin (DCX)	Rabbit	Abcam (**ab18723**)	1/500

analysis, neurospheroid sections were permeabilized for 30 min (10% milk solution [Sigma] in tris-buffered saline [TBS]). Primary antibodies were diluted in 10% milk solution (Sigma) in TBS and were incubated overnight at 4 °C (Table 2). Following washing, secondary antibody incubation was done for 1 h at RT. Antibodies used were: donkey anti-rabbit Alexa fluor 488 (1:600, A11006, ThermoFisher Scientific), donkey anti-rabbit Alexa fluor 555 (1:600, A11004, ThermoFisher Scientific), and goat anti-guinea pig Alexa fluor 555 (1:600, A11077, Invitrogen). DAPI was used to counterstain cellular nuclei. Pictures were taken using an Axioscan 7 microscope slide scanner (Zeiss).

Fluorescence quantification

The original, unedited pictures were used for quantification. Representative images were digitally enhanced to improve readability (contrast and brightness). Quantification of histopathological parameters was performed as described previously by investigators blinded to experimental groups [2,3[. To quantify lesion size ($GFAP^-$ area) and demyelinated area (MBP^- area), 5–7 10 μm thick sections per animal were obtained, whereby the lesion center and consecutive rostral and caudal area were analyzed. An intensity analysis was performed to determine astrogliosis (GFAP expression) using ImageJ [2]. To assess neuronal cell death at the lesion site, we quantified the number of cells positive for both cleaved caspase 3 and NeuN markers. This counting was performed in both the rostral and caudal regions relative to the lesion epicenter. The obtained values were normalized by the total number of $NeuN^+$ cells. Similarly, to quantify oligodendrocyte differentiation, cells positive for Olig2 and CC1 were counted using ImageJ in both rostral and caudal regions relative to the injury. The results were normalized by the total number of $Olig2^+$ cells. For evaluating serotonergic 5-HT regrowth, the rostral and caudal white matter regions of the ventral funiculus were analyzed for the amount of descending $5\text{-}HT^+$ fibers. T helper cells, identified as $CD4^+Iba\text{-}1^-$, were quantified by counting their number in one microscope field both rostral and caudal of the lesion site [30]. Differences in cleaved caspase, NeuN, and DCX positive cells within the neurospheroids were determined by intensity analysis using ImageJ, after which the positive area for each marker was corrected for the number of nuclei (based on the DAPI count) present in the pictures.

IncuCyte live-cell imaging of cleaved caspase 3/7

eGFP/Luc human iPSC-NSCs were seeded at a density of 1×10^4 cells per well in a Geltrex (Life Technologies) coated 96-well plate (flat bottom, Greiner). After allowing attachment for 24 h, cells were treated with the PDE4 inhibitors (vehicle: 0.1% DMSO; roflumilast: 1 μM; A33: 1 μM; Gebr32a: 1 μM), and apoptosis was induced by oxygen deprivation using a hypoxic chamber (1% O_2 for 4 h). Simultaneously, the IncuCyte Caspase-3/7 Red apoptosis reagent (1.5 μM; #4704, Sartorius) was supplemented to the cultures. Cell plates were placed into the IncuCyte live-cell analysis system, and 5 images were taken per well. End-point apoptosis was measured 6 h after oxygen deprivation. The IncuCyte integrated analysis software was used to quantify the total level of apoptosis.

Statistics

Data were analyzed using GraphPad Prism version 9 (GraphPad Software). All data were checked for normality using the Shapiro-Wilk test. The BMS scores, GFAP intensity and neurospheroid bioluminescent results were analyzed using a two-way ANOVA for repeated measurements with a Bonferroni post hoc test. Normally distributed data were subsequently analyzed with a one-way ANOVA with Dunnett's multiple comparisons (compared to vehicle). Not normally distributed data were tested using the non-parametric Kruskal-Wallis test with Dunn's multiple comparisons (compared to vehicle). Data are presented as mean ± standard error of the mean (SEM). Differences with P values < 0.05 were considered significant.

Results

Pan PDE4 and selective PDE4D, but not PDE4B, inhibition improve functional recovery and histopathological outcomes after SCI

Initially, we examined whether selective PDE4B or PDE4D inhibitors could improve functional recovery in a hemisection model of SCI. As a positive control, we included roflumilast, a second-generation pan PDE4 inhibitor. Starting 1 h post SCI injury, mice received either vehicle (DMSO) or the different PDE4 inhibitors: the pan PDE4 inhibitor roflumilast, the selective PDE4B inhibitor A33, the selective PDE4D inhibitor Gebr32a, or a sequential administration of A33 (1–9 dpi) followed by Gebr32a (10–28 dpi) to evaluate possible additive effects. Functional recovery was measured for 4 weeks using the BMS score. Both roflumilast and Gebr32a significantly improved functional recovery compared to vehicle-treated mice, whereas A33 treatment did not show any significant effect (Fig. 1A and B). Noteworthy, Gebr32a had a similar recovery profile as roflumilast (Fig. 1A and B). The sequential treatment with A33, followed by Gebr32a showed the same trend in functional recovery as Gebr32a treatment alone, namely starting from day 10, functional recovery of these mice mimicked the curve of the continuous Gebr32a treatment (Fig. 1A and B).

To further elucidate the clinical translatability of PDE4D inhibition, we administered Gebr32a starting 2 dpi which is considered a more clinically relevant treatment window. In addition, as the sequential treatment (A33 followed by Gebr32a after 10 dpi) resembled the results of Gebr32a treatment alone (Fig. 1A), we included a new treatment group where Gebr32a was administered alone starting 10 dpi to elucidate whether therapeutic efficacy is maintained without the preceding A33 treatment. Inhibition of PDE4D with Gebr32a, starting 2 dpi significantly improved functional recovery compared to vehicle-treated mice. However, starting Gebr32a treatment 10 dpi had no significant therapeutic benefit compared to vehicle treatment observed in the BMS scores but showed a significantly higher area under the curve compared to vehicle (Fig. 2A and B). Notably, the administration of Gebr32a 1 h after injury appeared to have a more pronounced improvement in the BMS score compared to Gebr32a treatment starting 2 dpi (Gebr32a start 1 h pi 3.93 ± 0.43 vs Gebr32a start 2 dpi 3.13 ± 0.29).

Histological GFAP and MBP analyses indicated significantly reduced lesion size and demyelinated areas, respectively, in roflumilast- and Gebr32a-treated mice compared to the vehicle group whereas the treatment with A33 was ineffective (Fig. 3A–J). Next, the level of astrogliosis was determined by analyzing GFAP intensity at varying distances to the lesion center. Whereas roflumilast and Geb32a treatment did not alter GFAP intensities, A33 exacerbated astrogliosis, especially at the rostral lesion site (Fig. 4A–E). As an additional neuroinflammatory outcome measurement, we determined the number of infiltrated $CD4^+$ T lymphocytes in the perilesional area. However, no differences between vehicle and treatment groups were observed (Supplementary Fig. S1).

Pan PDE4 and selective PDE4D inhibition increase the number of differentiated oligodendrocytes at the (peri)lesion site following SCI, unlike PDE4B inhibition

Due to the reduced demyelinated area observed at the lesion site upon both PDE4 and PDE4D inhibition, we next investigated the presence of differentiated oligodendrocytes ($CC1^+$) at the lesion site. The total number of oligodendrocyte lineage cells was first determined based on sole Olig2 positivity at the lesion site, which was unaltered upon either pan PDE4 or PDE4 subtype-selective inhibition compared to vehicle-

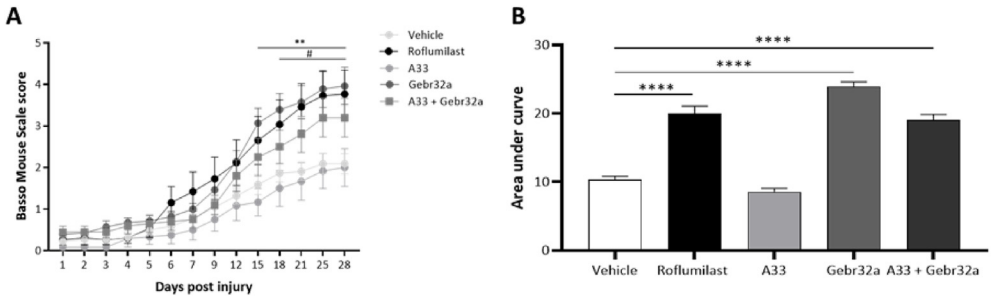

Fig. 1. Treatment with the PDE4 inhibitor roflumilast or the PDE4D inhibitor Gebr32a improve functional recovery after spinal cord injury, whereas the PDE4B inhibitor A33 has no effect. (A–B) Starting 1 h after injury, mice were treated with vehicle, a general PDE4 inhibitor roflumilast (3 mg/kg), or gene-specific PDE4 inhibitors, A33 (3 mg/kg) and Gebr32a (0.3 mg/kg). In contrast to A33, roflumilast and Gebr32a significantly improved **(A)** functional outcomes, measured by the BMS score and **(B)** area under the curve, compared to vehicle-treated mice over time. Data were analyzed using a two-way ANOVA with Bonferroni multiple comparison test (compared to vehicle). Data are displayed as mean ± SEM. $n = 10–16$ mice/group. #p ≤ 0.05 vehicle versus roflumilast; **p < 0.01 vehicle versus Gebr32a.

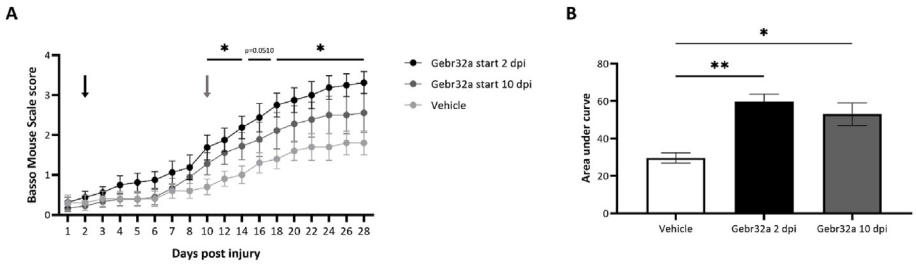

Fig. 2. Treatment with the PDE4D inhibitor Gebr32a starting 2 dpi, but not from 10 dpi, improves functional recovery after a spinal cord injury. (A–B) Starting directly after injury, mice were treated with vehicle. The Gebr32a treated animals changed from vehicle to Gebr32a (0.3 mg/kg) at 2 dpi or 10 dpi, while the vehicle croup continued DMSO (0.1%) treatment until 28 dpi. (**A**) Starting Gebr32a treatment 2 dpi, but not 10 dpi, significantly improved functional outcomes, measured by the BMS score. The black, and gray arrows indicate the start of Gebr32a treatment 2 dpi and 10 dpi, respectively. **(B)** Starting at 2 dpi and 10 dpi with Gebr32a significantly improved the area under the curve, compared to vehicle-treated mice over time. Data were analyzed using a two-way ANOVA with Bonferroni multiple comparison test (compared to vehicle). Data are displayed as mean ± SEM. $n = 5–9$ mice/group. **(A)** *p ≤ 0.05 Gebr32a start 2 dpi vs vehicle; **(B)** *p < 0.05, **p < 0.01 compared to vehicle.

treated animals (Supplementary Fig. S2). However, mice treated with roflumilast or Gebr32a did display a significant higher number of mature oligodendrocytes ($CC1^+Olig2^+$) compared to vehicle- or A33-treated animals (Fig. 5A–E).

Pan PDE4 and selective PDE4D inhibition is neuroprotective and stimulates 5-HT serotonergic regrowth after SCI, unlike PDE4B inhibition

Next, we investigated whether the abovementioned decreased lesion size was accompanied by neuroprotection and neuroregeneration. First, the neuroprotective effects of pan PDE4 or PDE4 subtype-selective inhibition were determined based on Cleaved Caspase 3 and NeuN double positivity at the lesion site to evaluate the number of apoptotic neurons. Mice treated with the pan PDE4 inhibitor roflumilast or the selective PDE4D inhibitor Gebr32a displayed a reduced number of Cleaved Caspase 3^+ $NeuN^+$ double positive cells compared to vehicle-treated animals at the (peri-)lesion (Fig. 6A–E). Furthermore, A33-treated animals displayed a trend ($p = 0.08$) toward reduced neuronal cell death (Fig. 6A–E).

Next, to determine the spinal dendritic plasticity of serotoninergic fiber projections, the number of descending 5-HT positive tracts was determined. In comparison with A33, both roflumilast- and Gebr32a-treated animals showed significantly increased mean number of descending 5-HT dendrites, indicating serotonergic neuroregeneration or protection (Fig. 7A and B).

Pan PDE4 and selective PDE4D inhibition prevents apoptosis of primary murine neurons and human iPSC-derived neural stem cells, unlike PDE4B inhibition

To evaluate whether the neuroprotection by roflumilast and Gebr32a observed *in vivo* could be attributed to direct neural protection, we assessed the effects of these PDE4 inhibitors on neural apoptosis in both primary mouse-derived neurons and human iPSC-derived NSCs. Fig. 8A shows the level of neuronal apoptosis of mouse neurons following 48 h of B27 growth factor deprivation. Both roflumilast-mediated PDE4 inhibition and Gebr32a-mediated PDE4D inhibition partly prevented the stress-induced neuronal apoptosis as observed by a higher PI signal compared to vehicle-treated cultures (Fig. 8A). Similarly, human iPSC-derived neural stem cell cultures subjected to oxygen deprivation for 4 h and treated with either roflumilast or Gebr32a displayed a significant reduction of Cleaved Caspase 3/7 positivity 6 h post stress-induced neural apoptosis (Fig. 8B).

Real-time bioluminescence monitoring of human neurospheroids demonstrates the neuroprotective feature of both pan PDE4 and selective PDE4D inhibition, which is accompanied by increased neuronal differentiation

To enable real-time read-out of neurospheroid viability, we used an eGFP/Luc human iPSC-derived neural stem cells stably expressing the

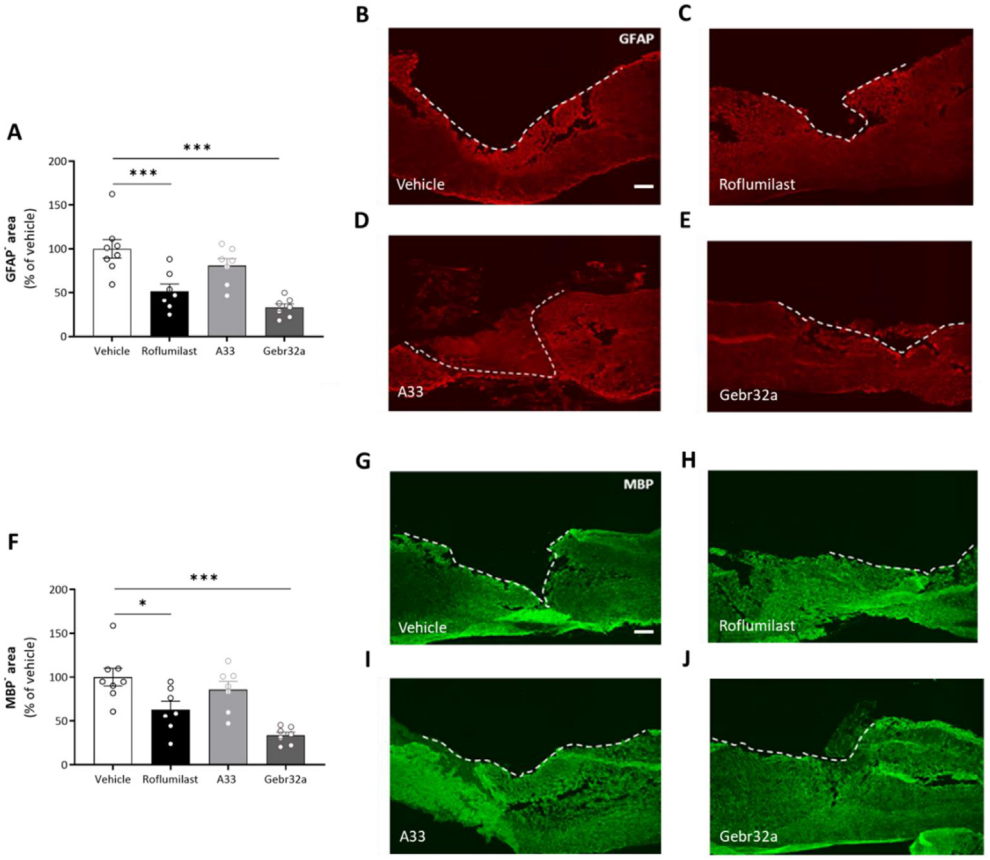

Fig. 3. Roflumilast or Gebr32a treatments reduce the lesion size and demyelinated area after spinal cord injury, whereas A33 has no effect. **(A–J)** Starting 1 h after injury, mice were treated with vehicle, the pan PDE4 inhibitor roflumilast (3 mg/kg), or the subtype-selective PDE4 inhibitors, A33 (3 mg/kg) and Gebr32a (0.3 mg/kg). **(A)** Quantification of lesion size, determined by the GFAP negative area, showed that this was reduced in mice treated with roflumilast or Gebr32a compared to the vehicle group. No difference between the vehicle and A33 groups was observed. Data were normalized to vehicle and are shown as mean ± SEM. n = 7–8 mice/group. **(B–E)** Representative images from the spinal cord sections are shown. Lesion size ($GFAP^-$ area) was determined as depicted by the dotted white line. Scale bar = 250 µm. **(F)** Quantification of the demyelinated area, determined by the MBP negative area, showed that this was reduced in mice treated with roflumilast or Gebr32a compared to the vehicle group. No difference between vehicle and A33 groups was observed. Data were normalized to vehicle and are shown as mean ± SEM. n = 7–8 mice/group. **(G–J)** Representative images from the spinal cord sections are shown. Demyelinated area (MBP^- area) was determined as depicted by the dotted white line. Scale bar = 250 µm. Demyelination area and lesion size were analyzed using a one-way ANOVA with Dunnett's multiple comparison test (compared to vehicle), *p < 0.05, ***p < 0.005. Data are displayed as mean ± SEM.

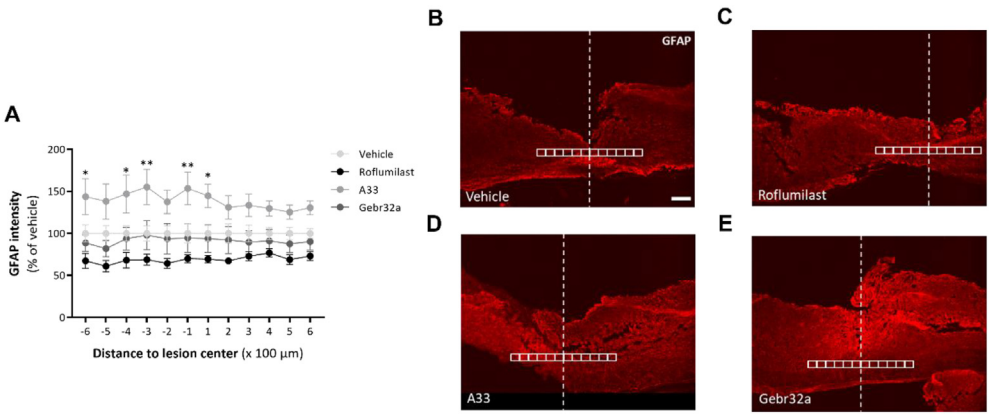

Fig. 4. Roflumilast and Gebr32a treatment do not affect astrogliosis after spinal cord injury, whereas A33 administration exacerbates astrocyte reactivity. **(A–E)** Starting 1 h after injury, mice were treated with vehicle, a pan PDE4 inhibitor roflumilast (3 mg/kg), or subtype-selective PDE4 inhibitors, A33 (3 mg/kg) and Gebr32a (0.3 mg/kg). **(A)** Quantification of astrogliosis by GFAP intensity analysis showed that, in contrast to other treatment groups, A33 application exacerbated astrogliosis compared to vehicle-treated mice. Data are shown as mean ± SEM. n = 4–6 mice/group. GFAP intensity was analyzed using a two-way ANOVA with a Bonferroni post hoc test. *p < 0.05 A33 versus vehicle, **p < 0.01 A33 versus vehicle. **(B–E)** Representative images from the spinal cord sections are shown. All analyses were quantified within square areas of 100 µm × 100 µm perilesional placed as indicated in the figure, extending 600 µm rostral to 600 µm caudal from the lesion center (white line). Scale bar = 500 µm.

firefly luciferase reporter. Over time, decreased viability was observed in the neurospheroids due to oxygen/nutrient deprivation in the core (Fig. 9A). In contrast to the selective PDE4B inhibitor A33, treatment with either the pan PDE4 inhibitor roflumilast or the selective PDE4D inhibitor Gebr32a stabilized neurospheroid viability when stress-induced core cell loss occurred (Fig. 9A). Of note, the overall size of the neurospheroids was not different between treatment groups (Fig. 9B). At the end of the 6-week culture period, neurospheroids were characterized for the level of apoptosis (Cleaved Caspase 3), neuronal differentiation (NeuN), and neurogenesis (DCX). Quantification of the Cleaved Caspase 3^+ area revealed a significant reduction in apoptosis when inhibiting PDE4 or PDE4D (Fig. 9C–F). Furthermore, both roflumilast and Gebr32a treatment significantly increased neuronal differentiation as more $NeuN^+$ cells were present at the end of the experiment (Fig. 9D–F). At end

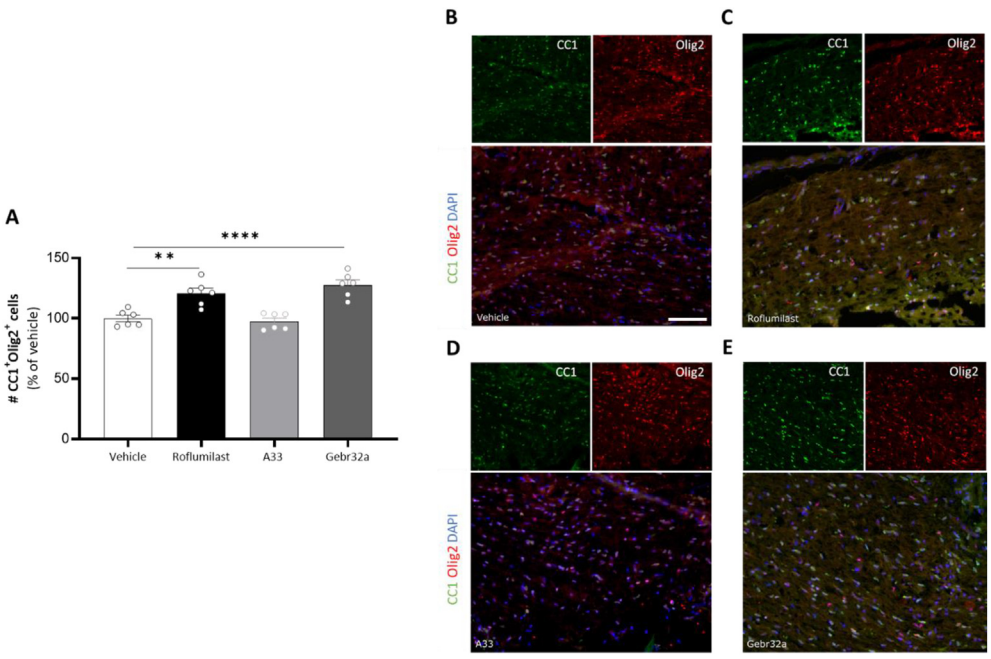

Fig. 5. Roflumilast and Gebr32a treatments increase the amount of mature oligodendrocytes at the peri-lesion site after spinal cord injury. (A–E) Starting 1 h after injury, mice were treated with vehicle, the pan PDE4 inhibitor roflumilast (3 mg/kg), or the subtype-selective PDE4 inhibitors, A33 (3 mg/kg) and Gebr32a (0.3 mg/kg). **(A)** Using a double staining for Olig2 (oligodendrolineage marker) and CC1 (mature oligodendrocyte marker), we showed a significantly increased percentage of mature oligodendrocytes at the lesion site following PDE4 (roflumilast) and PDE4D (Gebr32a) inhibition. n = 7–8 mice/group. Data were normalized to vehicle and are shown as mean ± SEM. Results were analyzed using a one-way ANOVA with Dunnett's multiple comparison test (compared to vehicle), **p < 0.01, ****p < 0.001. **(B–E)** Representative images of the Olig2-CC1 double staining at the lesion site. Single stainings are shown above the merged image. Scale bar = 100 µm.

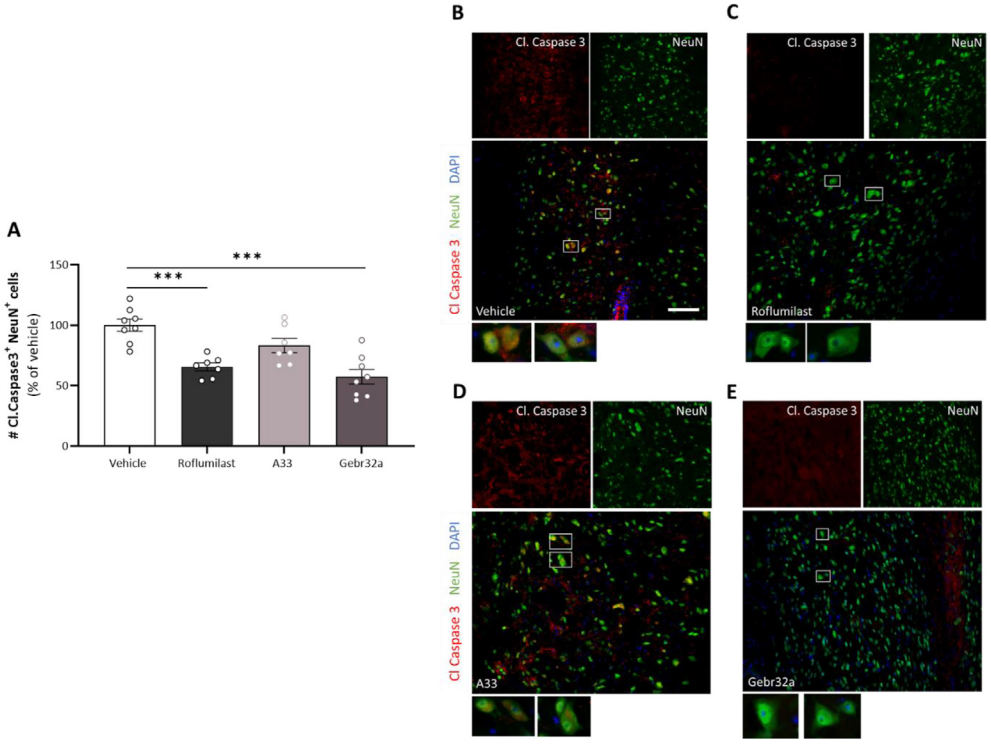

Fig. 6. Roflumilast and Gebr32a treatment act neuroprotective at the lesion site after spinal cord injury. (A–E) Starting 1 h after injury, mice were treated with vehicle, the pan PDE4 inhibitor roflumilast (3 mg/kg), or the subtype-selective PDE4 inhibitors, A33 (3 mg/kg) and Gebr32a (0.3 mg/kg). **(A)** Quantification of the number of Cleaved Caspase $3^{+}NeuN^{+}$ neurons at the (peri)lesion site indicated a neuroprotective effect of both PDE4 and PDE4D inhibition as reduced neuronal apoptosis was observed. n = 7–8 mice/group. Data are normalized to vehicle and are shown as mean ± SEM. Results were analyzed using a one-way ANOVA with Dunnett's multiple comparison test (compared to vehicle), ***p < 0.005. **(B–E)** Representative images of the Cleaved Caspase 3 NeuN staining at the lesion site. Single stainings are shown above the merged image. The white boxed regions are shown at higher magnification (40×) underneath the merged image. Scale bar = 100 µm.

stage, no significant differences were found in DCX^{+} area, nor for A33 treatment within any marker evaluated (Fig. 9E and F).

Discussion

In SCI research, PDE4 inhibition has yielded promising results due to its broad effects on different secondary injury-related outcomes, such as immune cell infiltration, inflammation, and axonal sprouting [8–11,31]. However, the clinical translation of pan-PDE4 inhibitors remains limited due to their poor tolerability in patients at doses required for clinical effectiveness [32]. In order to circumvent this pitfall, we investigated the potential of specific non-emetic PDE4B and PDE4D inhibitors, respectively A33 and Gebr32a. We now show that the PDE4D inhibitor Gebr32a significantly improved functional recovery after SCI similarly to the pan PDE4 inhibitor roflumilast, whereas the PDE4B inhibitor A33 did not. Moreover, starting Gebr32a at a more clinically relevant therapeutic window (2 dpi) still promoted functional recovery. In addition, both roflumilast and Gebr32a reduced the lesion size, demyelinated area, and

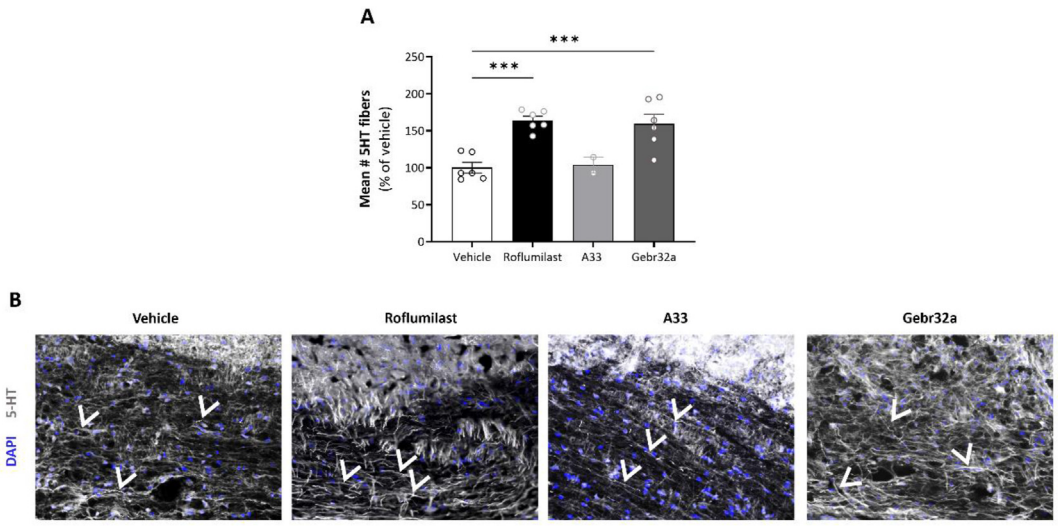

Fig. 7. Roflumilast and Gebr32a induce 5-HT serotonergic regrowth following SCI as indicated by the increased number of descending 5-HT tracts over the lesion site. **(A–B)** Starting 1 h after injury, mice were treated with vehicle, the pan PDE4 inhibitor roflumilast (3 mg/kg), or the subtype-specific PDE4 inhibitors, A33 (3 mg/kg) and Gebr32a (0.3 mg/kg). **(A)** Quantification of the 5-HT serotonergic staining showed an increase in the number **(A)** of descending 5-HT tracts over the SCI lesion site upon PDE4 (roflumilast) and PDE4D (Gebr32a) inhibition. Data were normalized to vehicle and are shown as mean ± SEM. n = 4–9 mice/group. **(B)** Representative images of the 5-HT staining at the lesion site. The white arrows indicate examples of 5-HT descending tracts. Results were analyzed using a one-way ANOVA with Dunnett's multiple comparison test (compared to vehicle), ***$p < 0.005$.

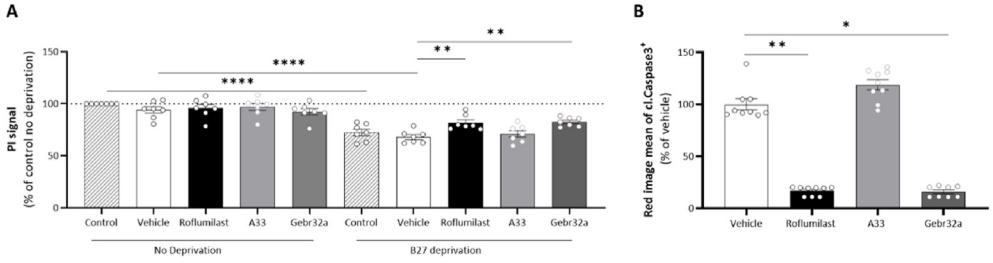

Fig. 8. Apoptosis of primary mouse neurons and human iPSC-derived NSCs was prevented by both roflumilast and Gebr32a treatment. **(A)** Primary mouse neurons deprived of the growth factor B27 for 48 h showed a decreased neuronal viability at the end of the experiment, which was partly prevented by inhibiting PDE4 (roflumilast, 1 μM) or PDE4D (Gebr32a, 1 μM). Data were normalized to vehicle and are shown as mean ± SEM. n = 6–7/group with an 'n' representative for one well. PI measurements of primary mouse neurons were analyzed using a one-way ANOVA with Dunnett's multiple comparison test (compared to vehicle). **(B)** Human iPSC-derived neural stem cells showed increased levels of Cleaved Caspase 3/7 upon oxygen deprivation, which was significantly reduced upon PDE4 (roflumilast, 1 μM) and PDE4D (Gebr32a, 1 μM) inhibition. n = 8–9/group with an 'n' representative for one well. Cleaved Caspase 3/7 signal measurements were analyzed using a non-parametric Kruskal-Wallis test with Dunn's multiple comparison test (compared to vehicle), *$p < 0.05$, **$p < 0.01$, ****$p < 0.001$. Data are displayed as mean ± SEM.

neuronal apoptosis while increasing the number of mature oligodendrocytes, and 5-HT$^+$ serotonergic fibers. The neuroprotective feature of both pan PDE4 inhibition and PDE4D subtype inhibition can be partially attributed to a direct neur(on)al effect as we showed a decreased neur(on)al apoptosis *in vitro* using murine neurons and iPSC-derived 3D neurospheroid cultures, which is in line with the previously described neuroplasticity enhancing properties of PDE4D inhibition [33]. These results support the use of the PDE4D inhibitor Gebr32a for SCI therapy.

We confirm that the second-generation PDE4 inhibitor roflumilast promoted SCI recovery, as demonstrated previously [34]. This second-generation PDE4 inhibitor is accompanied with less emetic side effects compared to first-generation pan-PDE4 inhibitors (e.g., rolipram) [35,36]. Noteworthy, the second-generation PDE3, PDE4, and PDE5 inhibitor Ibudilast is currently being evaluated for degenerative cervical myelopathy, a non-traumatic SCI [37]. However, translation of the roflumilast dose to promote CNS repair from rodents to humans, results in a dose approximately 500 times higher than the approved dose for roflumilast in chronic obstructive pulmonary disease. Hence, the CNS repair-inducing dose is still emetic [38]. Therefore, research to safer and more targeted options are crucial to influence discrete cell processes and promote SCI outcomes. Previous studies showed that PDE4B orchestrates the inflammatory immune response, while PDE4D contributes to adult neurogenesis, neuroplasticity, and myelin regeneration [39]. As SCI is characterized by a robust neuroinflammatory response and limited

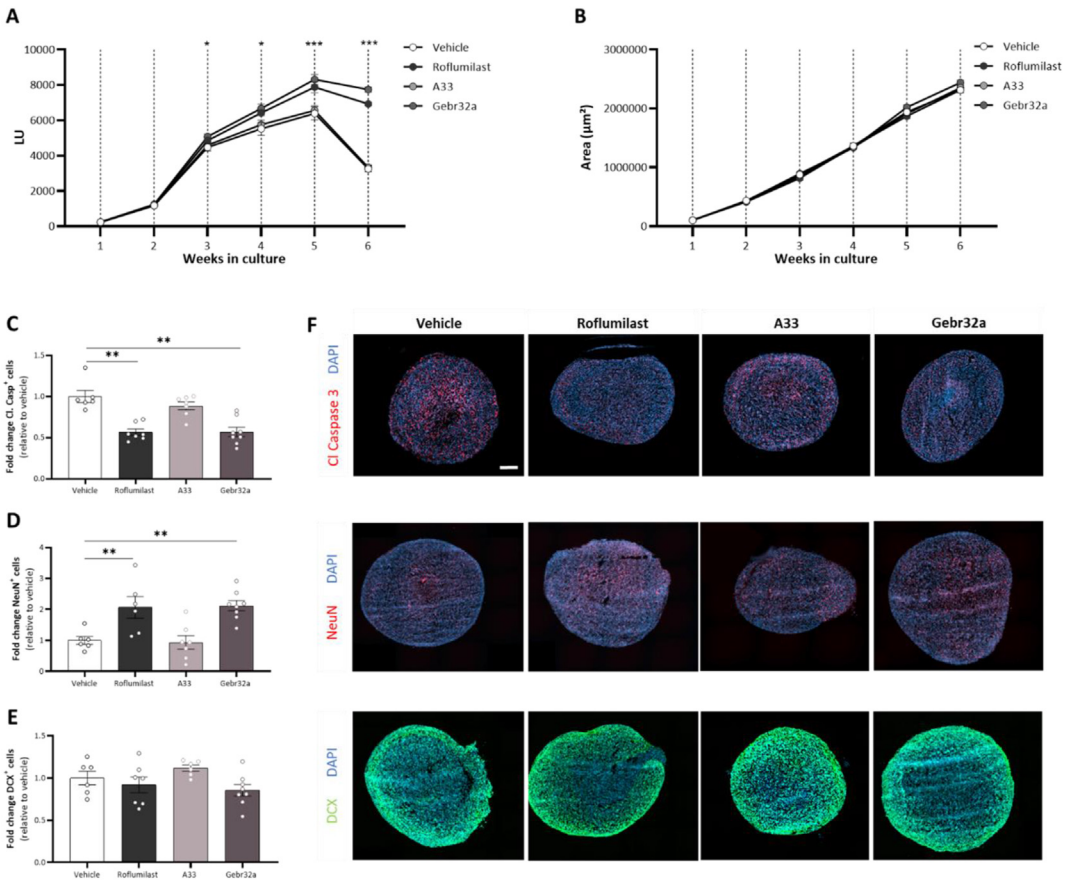

Fig. 9. Roflumilast and Gebr32a treatment protected human iPSC-derived neurospheroids from neural apoptosis and stimulated neuronal differentiation, while not affecting neurogenesis. **(A)** Weekly luminescence measurement of neurospheroids showed a stabilized viability over time, which decreased at 6 weeks of culture. However, this decrease was counteracted by treatment with roflumilast (1 µM) or Gebr32a (1 µM). **(B)** The size of the neurospheroids was not different between groups. **(A, B)** Data are shown as mean ± SEM. $n = 24$ spheroids/group. Data were analyzed using a two-way ANOVA with Dunnets multiple comparison test (compared to vehicle), *p < 0.05, ***p < 0.005. **(C–F)** At the end of the culture experiment, the 6-week-old neurospheroids were stained and quantified for **(C)** Cleaved Caspase 3 (apoptosis), **(D)** NeuN (neuronal differentiation), or **(E)** DCX (neurogenesis) positive cells with respect to the total number of nuclei. Data were normalized to vehicle and are shown as mean ± SEM. $n = 6–8$ spheroids/group. The amount of cleaved caspase positive cells was analyzed using a non-parametric Kruskal-Wallis test with Dunn's multiple comparisons (compared to vehicle). The amount of NeuN or DCX positive cells was analyzed using a one-way ANOVA with Dunnett's multiple comparison test (compared to vehicle), **p < 0.01. **(F)** Representative immunofluorescent images of the human iPSC-derived neurospheroids. Scale bar = 500 µm.

axonal regeneration, we focused on PDE4B and PDE4D inhibition. Important to note is that the inhibitors used in this study (A33 and Gebr32a) both lack an emetic response up to 100 mg/kg in animals, highlighting the clinical relevance of the evaluated compounds [38].

After SCI, PDE4B is acutely upregulated in the damaged spinal cord, especially in phagocytes [40]. The PDE4B subfamily is an important modulator of the intracellular cAMP levels in inflammatory cells, including macrophages, microglia, and astrocytes [5,14]. In a mouse model of multiple sclerosis, the PDE4B expression in antigen-presenting cells, such as phagocytes, was correlated with the disease severity [41]. Pharmacological inhibition of PDE4B by 0.3 mg/kg A33 i.p. administered 30 min after traumatic brain injury induction, induced anti-inflammatory markers (e.g., Arginase-1) in phagocytes and limited lesion size [42–44]. Complete PDE4B knockdown had beneficial effects on recovery in a contusion SCI model [40]. Based on these data, it was somewhat surprising that PDE4B inhibition by 3 mg/kg A33 (s.c) did not improve functional or histopathological recovery in our study. Moreover, PDE4B inhibition did exaggerate astrogliosis, which is considered detrimental for SCI outcomes since astrocytes contribute to the formation of the regenerative-limiting glial scar 45–48. Therefore, the absence of functional outcomes upon A33 treatment in our study could be attributed to the excessive astrogliosis. Importantly, it has been previously shown that treatment protocol and dose are important determinants for beneficial effects [49]. For example, intravenous (i.v.) or s.c. administration of the PDE4 inhibitor rolipram has been shown to be more effective to treat SCI compared to oral administration. Additionally, finetuning the PDE4 concentration showed to be crucial. More specifically, a low rolipram dose of 0.5 mg/kg/day had no beneficial effect for SCI treatment, while a higher dose of 1 mg/kg with the same treatment protocol could significantly improve SCI recovery [9]. However, an even higher dose of 0.8 mmol/kg/day demonstrated to not improve SCI recovery, postulated through off-target effects [10]. Therefore, performing a dose response study, testing another administration route, or different treatment timings can potentially result in ameliorated SCI outcomes upon A33 treatment. Hence, we cannot exclude that A33 could still provide long-term benefits after SCI. It is additionally crucial to highlight that the hemisection SCI model is highly effective for studying neuronal regeneration, but does not fully represent the human SCI pathology due to the lack of the complex neuroinflammatory responses. Conversely, the contusion SCI model provides a more faithful representation of neuroinflammation and axonal preservation evident in human SCI [50]. Consequently, it remains essential to consider the prospect that the anti-inflammatory attributes associated with the inhibition of PDE4B could potentially confer an indirect neuroprotective influence within the contusion SCI model. This warrants a thorough exploration when assessing the therapeutic viability of PDE4B inhibition within the

framework of the contusion SCI model.

Pan PDE4 inhibition using rolipram treatment after SCI has previously been shown to attenuate oligodendrocyte apoptosis and promote axonal growth and plasticity [4,49]. We have found that selective PDE4D inhibition by Gebr32a boosted oligodendrocyte precursor cell differentiation *in vitro* and stimulated remyelination in an *ex vivo* model [38]. In the current study, we show that Gebr32a administration, even when started 2 dpi, improved functional recovery after SCI. Previous research showed that earlier intervention results in better SCI outcomes [51,52]. Noteworthy, Gebr32a improved SCI outcomes significantly when administered in a clinically relevant therapeutic window but indeed, our results suggest that starting earlier with Gebr32a leads to better SCI outcomes (Gebr32a start 1 h pi 3.93 ± 0.43 vs Gebr32a start 2 dpi 3.13 ± 0.29). In mice treated 1 h post injury, we observed reduced lesion size and decreased demyelinated area, which was accompanied by increased numbers of mature oligodendrocytes, pointing toward reduced demyelination, mature oligodendrocyte protection or increased remyelination. Moreover, Gebr32a acts neuroprotective following SCI as demonstrated by the decreased number of apoptotic neurons. Previously, Gebr32a was shown to regulate neuronal morphology as demonstrated by the increased neurite outgrowth in both N2a and HT22 cells [13]. Due to this neuroregenerative feature of Gebr32a, combined with the observation that the loss of locomotor function following SCI correlates to the damage of 5-HT serotonergic projections in the spinal cord, we aimed to evaluate *in vivo* neuroregeneration by quantifying the descending 5-HT tracts over the lesion site [53]. Treatment of Gebr32a increased the number of descending 5-HT fibers, indicating either axonal sparing or neuroregenerative features of PDE4D inhibition. The effects observed after Gebr32a treatment were comparable to roflumilast. Although we cannot exclude any indirect neuroprotective effects of Gebr32a so far, we demonstrated here, at least partially, that the observed decrease in neuronal apoptosis can be attributed to direct neuronal protection. In both murine and human iPSC-derived neural stem cells, Gebr32a treatment diminished neur (on)al cell death. Similarly, Gebr32a stabilized the human neurospheroid viability, accompanied by decreased apoptosis and increased neuronal differentiation. Spinal cord neurons differ in calcium load, protection against reactive oxygen species, gene expression, and mitochondrial metabolism compared to brain-derived neurons, which suggests that spinal cord-derived neurons are more prone to trauma-induced injury [54–56]. Hence, validation of the neuroprotective and differentiation-stimulating effects of Gebr32a on spinal cord-derived neurons could be interesting for future research. Notably, previous research already demonstrated the neuroprotective effects of cAMP-elevating agents in spinal cord and brain-derived neurons [13,57,58]. Therefore, the neuroprotective effects and enhanced differentiation capacity upon Gebr32a administration in brain-derived cultures are proposed to translate toward spinal cord neurons.

Due to the hypothesized anti-inflammatory properties of PDE4B inhibition, and the previously observed regenerative properties of PDE4D inhibition, we evaluated whether a sequential treatment regimen could further improve SCI outcomes compared to monotreatment strategies. Thus, the PDE4B inhibitor A33 was administered during the initial phase of SCI and subsequently substituted by the PDE4D inhibitor Gebr32a from day 10 onwards. While inflammatory processes are essential for removing pathogens and cell debris, their benefits are overshadowed by the accumulation of inflammatory cytokines in the CNS upon inflammatory immune cell infiltration and activation [59,60]. These secondary inflammatory-mediated damage processes severely impair regenerative processes and glial functioning [61]. Therefore, by diminishing the neuroinflammatory response with PDE4B inhibition, we aimed to create a favorable micro-environment thereby allowing regeneration to occur more efficiently. By inhibiting PDE4D in a later phase, we hypothesized that the regenerative process could be further enhanced, and functional outcome would be improved even more compared to continuous PDE4B or PDE4D subtype inhibition throughout the disease course. However, in our model, inhibiting PDE4B by means of A33 during the early phase of the disease did not provide any additional benefit on functional outcome following hemisection SCI compared to continuous PDE4D inhibition by Gebr32a. However, when PDE4D inhibition was started 10 dpi, without preceding A33 administration, Gebr32a did not significantly ameliorate functional recovery, observed in the BMS scores. We propose that Gebr32a provides a therapeutic benefit when started 10 dpi, upon A33 treatment, due to the priming of A33 in the SCI environment. A33 can potentially create a more favorable CNS environment for neuronal repair, resulting in the therapeutic efficacy of Gebr32a when administered 10 dpi. Based on post-mortem analysis, A33 alone lacked efficacy which could be due to the dose, timing, route of administration or the harsh neurodegenerative conditions accompanied with a hemisection SCI lesion. Therefore, it cannot be excluded that sequential PDE4 subtype-specific treatment can be even more efficient and clinically relevant compared to only PDE4D inhibition to treat SCI.

Despite the promising preclinical findings on PDE4 inhibitors, the accompanied severe side effects at the therapeutic dose have hindered their clinical translation so far. In this study, we analyzed the impact of the PDE4B inhibitor A33 and the PDE4D inhibitor Gebr32a in a mouse model of SCI. In contrast to A33, Gebr32a improved functional recovery, even when treatment was initiated 2 dpi. In addition Gebr32a ameliorated histopathological outcomes to a comparable level as the pan PDE4 inhibitor roflumilast. Whereas roflumilast is associated with emetic-like side effects at its repair-inducing dose, Gebr32a is not. These data strongly support the notion that the selective PDE4D inhibitor Gebr32a holds great potential as a novel therapeutic approach for SCI treatment.

Funding

This study was supported by grants from Fonds Wetenschappelijk Onderzoek (FWO-Vlaanderen) to TVM, MS, SH, JVB, and FM (12G0817N, 1S57521N, G041421N, 1272324N, 1209123N, and 1SH2E24N). We also acknowledge partial funding from the University of Antwerp IOF-SBO brain organoid project granted to PP.

Author contributions

MS, SH, SL, NH, PP, JVB, and TV participated in the conceptualization, data interpretation and supervised the project. MS, FM, EvB, JVB carried out the investigation, and participated in data collection. MS, FM, and JVB wrote the manuscript. SH, EvB, PP, SL, NH, RR, EF, OB, CB, and JP reviewed the manuscript. All authors read and approved the final manuscript.

Declaration of competing interest

The authors declare the following financial interests/personal relationships which may be considered as potential competing interests: MS, JP, and TV have a proprietary interest in selective PDE4D inhibitors for the treatment of demyelinating disorders and neurodegenerative disorders. RR, EF, OB, CB, and JP have a proprietary interest in the use of Gebr32a. If there are other authors, they declare that they have no known competing financial interests or personal relationships that could have appeared to influence the work reported in this paper.

Acknowledgments

The authors would like to thank Dr. Leen Timmermans for her excellent technical assistance with the *in vivo* experiments.

Appendix A. Supplementary data

Supplementary data to this article can be found online at https://doi.org/10.1016/j.neurot.2024.e00372.

References

[1] Ren Y, Young W. Managing inflammation after spinal cord injury through manipulation of macrophage function. Neural Plast 2013;2013:945034.
[2] Van Broeckhoven J, Sommer D, Dooley D, Hendrix S, Franssen A. Macrophage phagocytosis after spinal cord injury: when friends become foes. Brain 2021; 144(10):2933–45.
[3] Tran AP, Warren PM, Silver J. The biology of regeneration failure and success after spinal cord injury. Physiol Rev 2018;98(2):881–917.
[4] Hannila SS, Filbin MT. The role of cyclic AMP signaling in promoting axonal regeneration after spinal cord injury. Exp Neurol 2008;209(2):321–32.
[5] Schepers M, Tiane A, Paes D, Sanchez S, Rombaut B, Piccart E, et al. Targeting phosphodiesterases-towards a tailor-made approach in multiple sclerosis treatment. Front Immunol 2019;10:1727.
[6] Zhou G, Wang Z, Han S, Chen X, Li Z, Hu X, et al. Multifaceted roles of cAMP signaling in the repair process of spinal cord injury and related combination treatments. Front Mol Neurosci 2022;15:808510.
[7] Paes D, Schepers M, Rombaut B, van den Hove D, Vanmierlo T, Prickaerts J. The molecular biology of phosphodiesterase 4 enzymes as pharmacological targets: an interplay of isoforms, conformational states, and inhibitors. Pharmacol Rev 2021; 73(3):1016–49.
[8] Bao F, Fleming JC, Golshani R, Pearse DD, Kasabov L, Brown A, et al. A selective phosphodiesterase-4 inhibitor reduces leukocyte infiltration, oxidative processes, and tissue damage after spinal cord injury. J Neurotrauma 2011;28(6):1035–49.
[9] Schaal SM, Garg MS, Ghosh M, Lovera L, Lopez M, Patel M, et al. The therapeutic profile of rolipram, PDE target and mechanism of action as a neuroprotectant following spinal cord injury. PLoS One 2012;7(9):e43634.
[10] Nikulina E, Tidwell JL, Dai HN, Bregman BS, Filbin MT. The phosphodiesterase inhibitor rolipram delivered after a spinal cord lesion promotes axonal regeneration and functional recovery. Proc Natl Acad Sci U S A 2004;101(23):8786–90.
[11] Whitaker CM, Beaumont E, Wells MJ, Magnuson DS, Hetman M, Onifer SM. Rolipram attenuates acute oligodendrocyte death in the adult rat ventrolateral funiculus following contusive cervical spinal cord injury. Neurosci Lett 2008; 438(2):200–4.
[12] Mussen F, Broeckhoven JV, Hellings N, Schepers M, Vanmierlo T. Unleashing spinal cord repair: the role of cAMP-specific PDE inhibition in attenuating neuroinflammation and boosting regeneration after traumatic spinal cord injury. Int J Mol Sci 2023;24(9).
[13] Paes D, Schepers M, Willems E, Rombaut B, Tiane A, Solomina Y, et al. Ablation of specific long PDE4D isoforms increases neurite elongation and conveys protection against amyloid-beta pathology. Cell Mol Life Sci 2023;80(7):178.
[14] Pearse DD, Hughes ZA. PDE4B as a microglia target to reduce neuroinflammation. Glia 2016;64(10):1698–709.
[15] Avila DV, Myers SA, Zhang J, Kharebava G, McClain CJ, Kim HY, et al. Phosphodiesterase 4b expression plays a major role in alcohol-induced neuro-inflammation. Neuropharmacology 2017;125:376–85.
[16] Jin SL, Lan L, Zoudilova M, Conti M. Specific role of phosphodiesterase 4B in lipopolysaccharide-induced signaling in mouse macrophages. J Immunol 2005; 175(3):1523–31.
[17] Shi Y, Lv J, Chen L, Luo G, Tao M, Pan J, et al. Phosphodiesterase-4D knockdown in the prefrontal cortex alleviates memory deficits and synaptic failure in mouse model of alzheimer's disease. Front Aging Neurosci 2021;13:722580.
[18] Sierksma AS, van den Hove DL, Pfau F, Philippens M, Bruno O, Fedele E, et al. Improvement of spatial memory function in APPswe/PS1dE9 mice after chronic inhibition of phosphodiesterase type 4D. Neuropharmacology 2014;77:120–30.
[19] Schepers M, Vanmierlo T. Novel insights in phosphodiesterase 4 subtype inhibition to target neuroinflammation and stimulate remyelination July 20. Neural Regeneration Research 2023;19(3):493–4.
[20] Van Broeckhoven J, Erens C, Sommer D, Scheijen E, Sanchez S, Vidal PM, et al. Macrophage-based delivery of interleukin-13 improves functional and histopathological outcomes following spinal cord injury. J Neuroinflammation 2022;19(1):102.
[21] Sommer D, Corstjens I, Sanchez S, Dooley D, Lemmens S, Van Broeckhoven J, et al. ADAM17-deficiency on microglia but not on macrophages promotes phagocytosis and functional recovery after spinal cord injury. Brain Behav Immun 2019;80: 129–45.
[22] Erens C, Van Broeckhoven J, Hoeks C, Schabbauer G, Cheng PN, Chen L, et al. L-arginine depletion improves spinal cord injury via immunomodulation and nitric oxide reduction. Biomedicines 2022;10(2).
[23] Ricciarelli R, Brullo C, Prickaerts J, Arancio O, Villa C, Rebosio C, et al. Memory-enhancing effects of GEBR-32a, a new PDE4D inhibitor holding promise for the treatment of Alzheimer's disease. Sci Rep 2017;7:46320.
[24] Basso DM, Fisher LC, Anderson AJ, Jakeman LB, McTigue DM, Popovich PG. Basso Mouse Scale for locomotion detects differences in recovery after spinal cord injury in five common mouse strains. J Neurotrauma 2006;23(5):635–59.
[25] Sciarretta C, Minichiello L. The preparation of primary cortical neuron cultures and a practical application using immunofluorescent cytochemistry. Methods Mol Biol 2010;633:221–31.
[26] Lo Monaco M, Gervois P, Beaumont J, Clegg P, Bronckaers A, Vandeweerd JM, et al. Therapeutic potential of dental pulp stem cells and leukocyte- and platelet-rich fibrin for osteoarthritis. Cells 2020;9(4).
[27] Evens L, Heeren E, Rummens JL, Bronckaers A, Hendrikx M, Deluyker D, et al. Advanced glycation end products impair cardiac atrial appendage stem cells properties. J Clin Med 2021;10(13).
[28] Van Breedam E, Nijak A, Buyle-Huybrecht T, Di Stefano J, Boeren M, Govaerts J, et al. Luminescent human iPSC-derived neurospheroids enable modeling of neurotoxicity after oxygen-glucose deprivation. Neurotherapeutics 2022;19(2): 550–69.
[29] Nelissen S, Vangansewinkel T, Geurts N, Geboes L, Lemmens E, Vidal PM, et al. Mast cells protect from post-traumatic spinal cord damage in mice by degrading inflammation-associated cytokines via mouse mast cell protease 4. Neurobiol Dis 2014;62:260–72.
[30] Dooley D, Lemmens E, Vangansewinkel T, Le Blon D, Hoornaert C, Ponsaerts P, et al. Cell-based delivery of interleukin-13 directs alternative activation of macrophages resulting in improved functional outcome after spinal cord injury. Stem Cell Rep 2016;7(6):1099–115.
[31] Butler MB, Vellaiyappan SK, Bhatti F, Syed FE, Rafati Fard A, Teh JQ, et al. The impact of phosphodiesterase inhibition on neurobehavioral outcomes in preclinical models of traumatic and non-traumatic spinal cord injury: a systematic review. Front Med 2023;10:1237219.
[32] Knott EP, Assi M, Rao SN, Ghosh M, Pearse DD. Phosphodiesterase inhibitors as a therapeutic approach to neuroprotection and repair. Int J Mol Sci 2017;18(4).
[33] Paes D, Lardenoije R, Carollo RM, Roubroeks JAY, Schepers M, Coleman P, et al. Increased isoform-specific phosphodiesterase 4D expression is associated with pathology and cognitive impairment in Alzheimer's disease. Neurobiol Aging 2021; 97:56–64.
[34] Moradi K, Golbakhsh M, Haghighi F, Afshari K, Nikbakhsh R, Khavandi MM, et al. Inhibition of phosphodiesterase IV enzyme improves locomotor and sensory complications of spinal cord injury via altering microglial activity: introduction of Roflumilast as an alternative therapy. Int Immunopharm 2020; 86:106743.
[35] Vanmierlo T, Creemers P, Akkerman S, van Duinen M, Sambeth A, De Vry J, et al. The PDE4 inhibitor roflumilast improves memory in rodents at non-emetic doses. Behav Brain Res 2016;303:26–33.
[36] Richter W, Menniti FS, Zhang HT, Conti M. PDE4 as a target for cognition enhancement. Expert Opin Ther Targets 2013;17(9):1011–27.
[37] Davies B, Mowforth OD, Yordanov S, Alvarez-Berdugo D, Bond S, Nodale M, et al. Targeting patient recovery priorities in degenerative cervical myelopathy: design and rationale for the RECEDE-Myelopathy trial-study protocol. BMJ Open 2023; 13(3):e061294.
[38] Schepers M, Paes D, Tiane A, Rombaut B, Piccart E, van Veggel L, et al. Selective PDE4 subtype inhibition provides new opportunities to intervene in neuroinflammatory versus myelin damaging hallmarks of multiple sclerosis. Brain Behav Immun 2023;109:1–22.
[39] Titus DJ, Wilson NM, Freund JE, Carballosa MM, Sikah KE, Furones C, et al. Chronic cognitive dysfunction after traumatic brain injury is improved with a phosphodiesterase 4B inhibitor. J Neurosci 2016;36(27):7095–108.
[40] Myers SA, Gobejishvili L, Saraswat Ohri S, Garrett Wilson C, Andres KR, Riegler AS, et al. Following spinal cord injury, PDE4B drives an acute, local inflammatory response and a chronic, systemic response exacerbated by gut dysbiosis and endotoxemia. Neurobiol Dis 2019;124:353–63.
[41] Sanabra C, Johansson EM, Mengod G. Critical role for PDE4 subfamilies in the development of experimental autoimmune encephalomyelitis. J Chem Neuroanat 2013;47:96–105.
[42] Wilson NM, Gurney ME, Dietrich WD, Atkins CM. Therapeutic benefits of phosphodiesterase 4B inhibition after traumatic brain injury. PLoS One 2017;12(5): e0178013.
[43] Ghosh M, Xu Y, Pearse DD. Cyclic AMP is a key regulator of M1 to M2a phenotypic conversion of microglia in the presence of Th2 cytokines. J Neuroinflammation 2016;13:9.
[44] Erdely A, Kepka-Lenhart D, Clark M, Zeidler-Erdely P, Poljakovic M, Calhoun WJ, et al. Inhibition of phosphodiesterase 4 amplifies cytokine-dependent induction of arginase in macrophages. Am J Physiol Lung Cell Mol Physiol 2006;290(3):L534–9.
[45] Silver J, Miller JH. Regeneration beyond the glial scar. Nat Rev Neurosci 2004;5(2): 146–56.
[46] Kanemaru K, Kubota J, Sekiya H, Hirose K, Okubo Y, Iino M. Calcium-dependent N-cadherin up-regulation mediates reactive astrogliosis and neuroprotection after brain injury. Proc Natl Acad Sci USA 2013;110(28):11612–7.
[47] Fawcett JW, Asher RA. The glial scar and central nervous system repair. Brain Res Bull 1999;49(6):377–91.
[48] Sofroniew MV. Molecular dissection of reactive astrogliosis and glial scar formation. Trends Neurosci 2009;32(12):638–47.
[49] Costa LM, Pereira JE, Filipe VM, Magalhaes LG, Couto PA, Gonzalo-Orden JM, et al. Rolipram promotes functional recovery after contusive thoracic spinal cord injury in rats. Behav Brain Res 2013;243:66–73.
[50] Sharif-Alhoseini M, Khormali M, Rezaei M, Safdarian M, Hajighadery A, Khalatbari MM, et al. Animal models of spinal cord injury: a systematic review. Spinal Cord 2017;55(8):714–21.
[51] Pedro KM, Fehlings MG. Time is spine: what's over the horizon. J Clin Orthop Trauma 2022;35:102043.
[52] Badhiwala JH, Ahuja CS, Fehlings MG. Time is spine: a review of translational advances in spinal cord injury. J Neurosurg Spine 2018;30(1):1–18.
[53] Perrin FE, Noristani HN. Serotonergic mechanisms in spinal cord injury. Exp Neurol 2019;318:174–91.
[54] Panov AV, Kubalik N, Zinchenko N, Ridings DM, Radoff DA, Hemendinger R, et al. Metabolic and functional differences between brain and spinal cord mitochondria underlie different predisposition to pathology. Am J Physiol Regul Integr Comp Physiol 2011;300(4):R844–54.

[55] Pfisterer U, Khodosevich K. Neuronal survival in the brain: neuron type-specific mechanisms. Cell Death Dis 2017;8(3):e2643.
[56] Liu Y, Zhou LJ, Wang J, Li D, Ren WJ, Peng J, et al. TNF-Alpha differentially regulates synaptic plasticity in the Hippocampus and spinal cord by microglia-dependent mechanisms after peripheral nerve injury. J Neurosci 2017;37(4):871–81.
[57] Montoya GJ, Sutachan JJ, Chan WS, Sideris A, Blanck TJ, Recio-Pinto E. Muscle-conditioned media and cAMP promote survival and neurite outgrowth of adult spinal cord motor neurons. Exp Neurol 2009;220(2):303–15.
[58] Aglah C, Gordon T, Posse de Chaves EI. cAMP promotes neurite outgrowth and extension through protein kinase A but independently of Erk activation in cultured rat motoneurons. Neuropharmacology 2008;55(1):8–17.
[59] Freyermuth-Trujillo X, Segura-Uribe JJ, Salgado-Ceballos H, Orozco-Barrios CE, Coyoy-Salgado A. Inflammation: a target for treatment in spinal cord injury. Cells 2022;11(17).
[60] Orr MB, Gensel JC. Spinal cord injury scarring and inflammation: therapies targeting glial and inflammatory responses. Neurotherapeutics 2018;15(3):541–53.
[61] Lin ZH, Wang SY, Chen LL, Zhuang JY, Ke QF, Xiao DR, et al. Methylene blue mitigates acute neuroinflammation after spinal cord injury through inhibiting NLRP3 inflammasome activation in microglia. Front Cell Neurosci 2017;11:391.